Chapter 4

Neutron capture cross section measurement for tungsten isotope in the neutron energy range 0.6 to 3.2 MeV

4.1 Introduction

In ITER-like fusion reactors, tungsten (W) consider as a prime materials used in First-wall and Plasma Facing Components (PFCs). Tungsten material has other applications like it is used as a target material in high-current accelerators and for neutron dosimetry via neutron capture $^{186}W(n,\gamma)$ reaction. The neutron capture cross section is also important in astrophysics applications [1-5]. In the present chapter, the neutron capture cross section measurement of ^{186}W-isotope is presented in the neutron energy range from 0.6 to 3.2 MeV. The measurement are done using the neutron activation analysis followed by offline γ-ray spectroscopy technique. The neutrons are produced from $^{7}Li(p,n)^{7}Be$ reaction. The neutron capture cross section for ^{186}W isotope is measured relative to $^{115}In(n,n'\gamma)^{115m}In$ monitor reaction cross section. The correction factors such as γ-ray self-absorption factor of the sample at a given γ-energy (C_s), the flux attenuation factor (C_a), the counting geometry factor (C_g) and correction in measured cross section due to lower energy neutrons are also presented in this chapter. The cross section measurements are also presented with the detailed covariance analysis and correlation matrix. The measured cross section are compared with the previously published cross section results [6-18]. The measured reaction cross section data has been compared with the theoretically calculated data based on TALYS-1.9 [19] and EMPIRE-3.2.2 [20] nuclear codes and with the evaluated data from ENDF/B-VIII.0, JEFF-3.3 and JENDL-5 [21-23].

4.2 Experimental Details

The experiments were performed at the 6-MV Folded Tandem Ion Accelerator (FOTIA) Facility, Nuclear Physics Division, Bhabha Atomic Research Centre (BARC), Mumbai [24]. The proton beam of energies 2.6, 4 and 5 MeV were incident onto a target foil

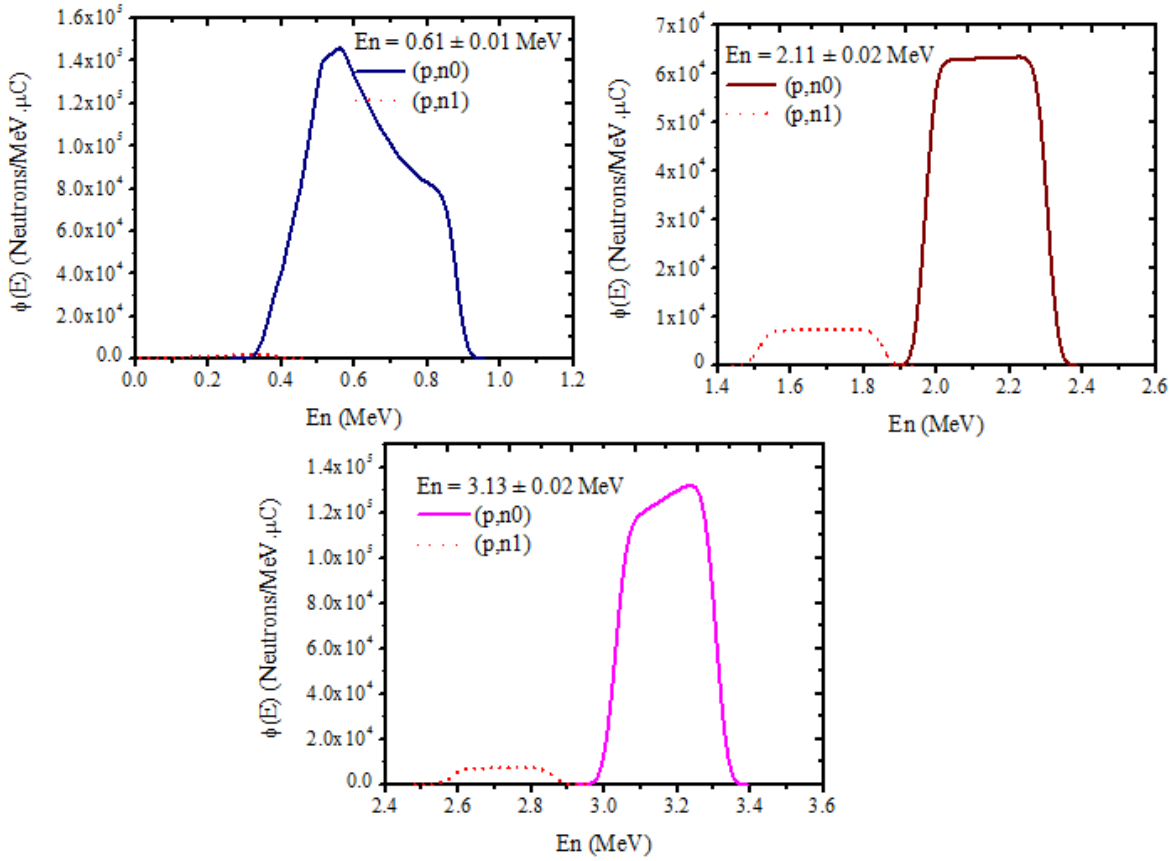

Figure 4.1 Neutron flux energy spectrum Φ(E), for (i) E_p = 2.6 MeV, (ii) E_p = 4.0 MeV and (iii) E_p = 5.0 MeV generated from EPEN code

of natural lithium (Li) with thickness of 4 mg/cm^2 to produce neutron beam through the ^{7}Li(p,n)^{7}Be reaction (E_{th}= 1.881 MeV). The proton beam has a spread of energy of ± 0.02 MeV, while the beam current fluctuates between 90-100 nA during irradiation. The neutron beam energy spectrum cannot be measured using the Time of Flight technique because of the continuous proton beam. The neutron flux energy spectrum Φ(E) from the ^{7}Li(p,n)^{7}Be reaction was obtained using the EPEN- (Energy of Proton Energy of Neutron) code which was utilized for the incident proton energies from the reaction threshold to 7 MeV [25, 26]. Since the proton energies were higher than the threshold energy of ^{7}Li(p,n)^{7}Be reaction in the present experiment, the second energy group of low energy neutrons from the ^{7}Li(p,n$_1$)^{7}Be* and ^{7}Li(p,n+^{3}He)^{4}He reactions will contribute in addition to the ^{7}Li(p,n$_0$)^{7}Be reaction. The correction due to the lower energy neutrons was discussed in Sub-Section 4.3.3. The neutron flux energy spectra Φ_0(E) determined from EPEN code for the proton energies (E_p) of 2.6, 4 and 5 MeV are shown in *Figure 4.1*. The neutron spectrum had a spread due to proton energy loss in the lithium target. The mean energy of the (p,n$_0$) neutron group was obtained by,

$$< E_n >= \frac{\int \Phi_0(E) E dE}{\int \Phi_0(E) dE} \quad (4.1)$$

Where, $\Phi_0(E)$ is the (p,n_0) neutron flux calculated by EPEN neutron flux energy spectra and the corresponding neutron energies are 0.61 ± 0.01, 2.11 ± 0.02 and 3.13 ± 0.02 MeV for E_p = 2.6, E_p=4 and E_p=5 MeV, respectively.

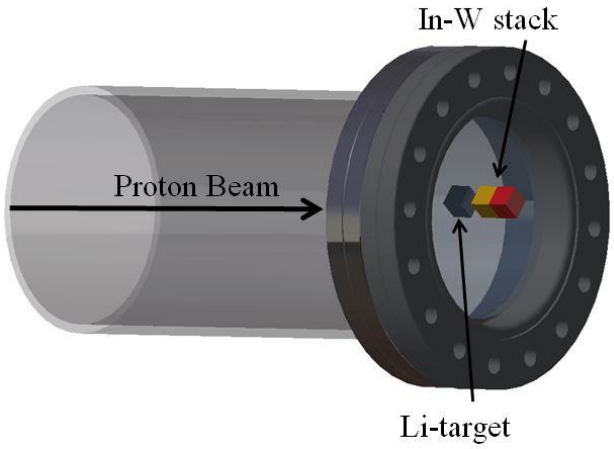

Figure 4.2 Schematic diagram of experimental set up for neutron irradiation

Table 4.1 Summary of experimental sample details

Isotope	Sample	Isotope Abundance (%)	E_n (MeV)	Thickness (cm)	Density (g/cm^3)	Weight of isotope in sample (mg)	Number of atoms (10^{-4} atoms/b)
^{186}W	W–foil	28.43(2)	0.61±0.01	0.01	19.23	283.4±0.1	2.639
			2.11±0.02			313.1±0.1	2.916
			3.13±0.02			299.2±0.1	2.783
^{115}In	In-foil	95.17(5)	0.61±0.01	0.05	7.31	250.1±0.1	12.545
			2.11±0.02			275.6±0.1	9.611
			3.13±0.02			257.0±0.1	12.891

Natural tungsten (W) metal foil of dimension 10×10× 0.1 mm^3 and natural indium (In) metal foil of dimension 10×10×0.5 mm^3 were used for the present experiment. They were wrapped separately with a 0.025 mm thick pure aluminium foil. The sample target with the monitor was

stacked as “In-W” and mounted one stack at a time in forward direction of the incident beam at a distance of 12 mm from Li foil. A schematic diagram of the irradiation set up as shown in *Figure 4.2* and the sample details are given in *Table 4.1.* The In-W stacks were irradiated with the neutron beam of energies 0.61 ± 0.01, 2.11 ± 0.02 and 3.13 ± 0.02 MeV, respectively.

4.3 Data analysis

4.3.1 Measurement of γ-ray activity

The In-W stacks were irradiated for six hours to generate sufficient activity in the samples. After each irradiation, the tungsten (W) target and indium (In) monitor samples were cooled for 1-2 hours. The cooled irradiated samples were mounted on different perspex plates and taken for offline γ-ray counting. The W samples were additionally cooled for 5-7 hours. The details of the irradiation, cooling and counting times are given in *Table 4.2.* The γ-ray counting was performed for a time period of 2-7 hours to obtain sufficient γ-ray activity to reduce the statistical errors. The measurement of the γ-ray activity of the reaction products was performed using a lead shielded 180cc High Purity Germanium (HPGe) detector with an efficiency of 30% and an energy resolution of 1.8 keV for 1332 keV γ-ray energy of ^{60}Co. The energy and efficiency calibration of the HPGe detector was performed by using a multi γ-ray source ^{152}Eu ($T_{1/2}$ = 13.517±0.0009 years) having activity of 6659.21±82 Bq on 1 October 1999 [27]. The recorded γ-ray spectrum of the reaction produced from the ^{186}W(n,γ)^{187}W reaction is shown in *Figure 4.3* along with a background spectrum. The recording and analysis of the γ-ray spectrum were performed using CAMAC-based LAMPS software. The nuclear spectroscopic data are taken from Refs. [28-30] and given in *Table 4.3.* The product nuclei ^{115m}In of the ^{115}In(n,n’) reaction emit 336.241 keV γ-ray energy whereas ^{187}W of the ^{186}W(n,γ) reaction emit 479.53 keV and 685.81 keV γ-ray energies. The photo-peak activity of 336.241 keV γ-ray energy of ^{115m}In was used to calculate the neutron flux, whereas 479.53 keV γ-ray energy of ^{187}W was used to estimate the ^{186}W(n,γ) reaction cross section.

Table 4.2 The Experimental details of irradiation

Reaction	E_n (MeV)	Irradiation time (sec)	Cooling time (sec)	Counting time (sec)
$^{115}In(n,n')^{115m}In$	0.61±0.01	21660	4420	1380
	2.11±0.02	21600	2018	1420
	3.13±0.02	21660	5056	1272
$^{186}W(n,\gamma)^{187}W$	0.61±0.01	21660	31832	18600
	2.11±0.02	21600	67183	27854
	3.13±0.02	21660	48340	12262

Table 4.3 Nuclear spectroscopic data of sample and monitor reactions

Reaction	Product nuclei	Half-life (hour)	E_γ (keV)	I_γ (%)
$^{115}In(n,n')$	^{115m}In	4.486 ± 0.004	336.241	45.9 ± 0.1
$^{186}W(n,\gamma)$	^{187}W	24.0 ± 0.4	479.53	26.6 ± 0.4
			685.81	33.2 ± 0.5

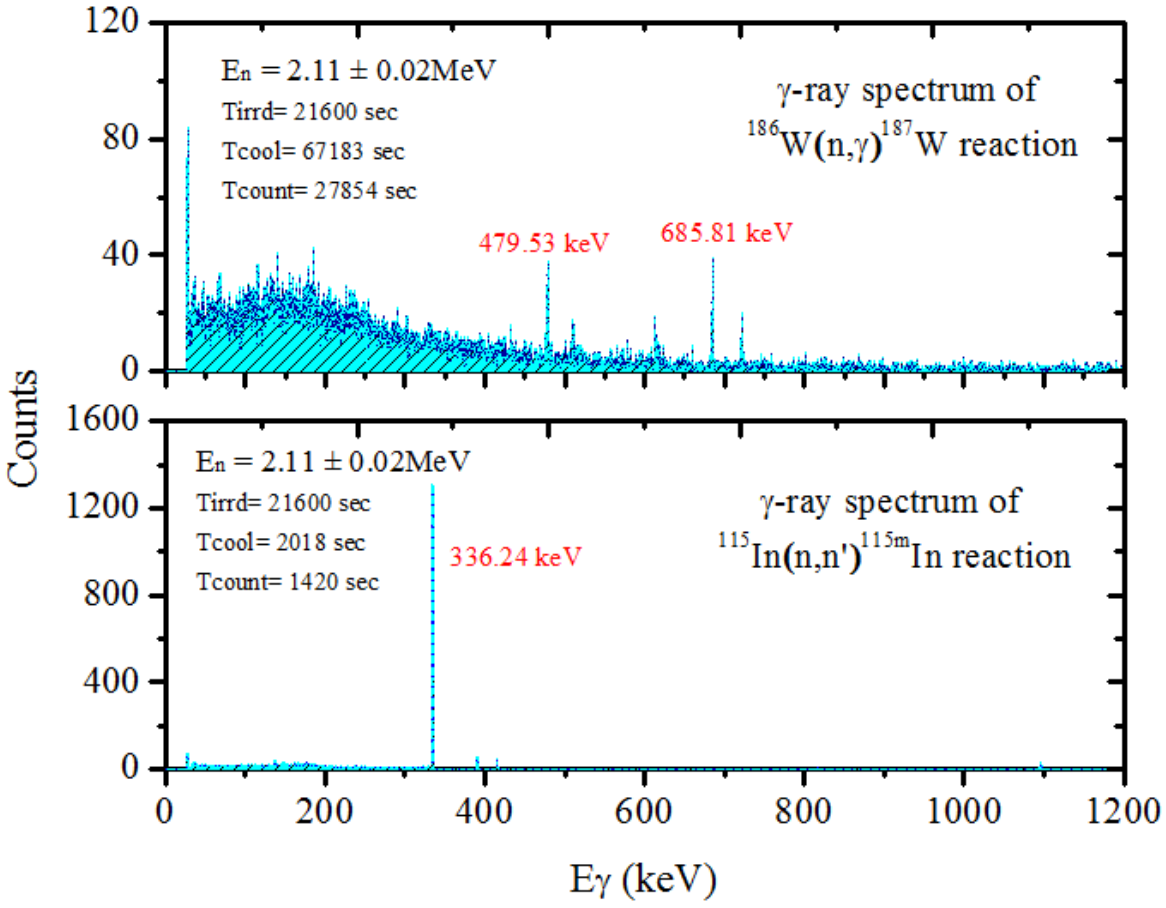

Figure 4.3 A typical γ-ray spectrum of $^{186}W(n,\gamma)^{187}W$ and $^{115}In(n,n')^{115m}In$ monitor reactions for E_n = 2.11 ± 0.02 MeV recorded by HPGe detector

The efficiency of the detector* at different γ-ray energies was determined by following relation.

$$\varepsilon = \frac{C_{obs}K_c}{A_o I_\gamma e^{-\lambda T} \nabla t} \tag{4.2}$$

Where, C_{obs} is the number of counts measured in time (Δt = 5485 sec), I_γ is the absolute intensity for a given γ-ray energy, A_0 is the activity of the ^{152}Eu-source at the time of fabrication, T is the time interval between fabrication of the source and the date of the experiment. K_c is the coincidence summing correction factor calculated by the Monte Carlo simulation code EFFTRAN [31]. The code required the material details and dimensions of the HPGe detector and calibration source [32, 33]. The detector efficiencies for the characteristic γ-ray energies of the ^{152}Eu source with correction factor (K_c) were given in *Table 4.4.* The measured efficiency and the corrected efficiency were compared in *Figure 4.4.*

* The details of efficiency calibration is summarized in Sub-Section 2.4.4.

Table 4.4 Details of HPGe detector efficiency with uncertainty for ^{152}Eu-source

E_γ (keV)	I_γ	*Counts (C_{obs})*	K_c	*Efficiency (ε)*	Δε
121.78	0.2853 ± 0.0016	336620 ± 461	1.165	0.101078	0.001632
344.27	0.2659 ± 0.0004	171402.4 ± 516.8	1.113	0.052850	0.000948
778.90	0.1294 ± 0.0008	36409.4 ± 336.3	1.165	0.024143	0.000452
964.07	0.1461 ± 0.0007	35981.7 ± 556.5	1.099	0.019945	0.000441
1085.86	0.1021 ± 0.0005	26751.6 ± 370.2	0.915	0.017665	0.000372
1408.01	0.2101 ± 0.0009	37819.5 ± 596.7	1.036	0.013741	0.000306

Covariance analysis and uncertainty propagation in detector efficiency

The efficiency of the characteristic γ-ray energies of the ^{187}W and ^{115m}In nuclides were determined by interpolating the point-wise efficiencies of the γ-ray energies given in *Table 4.4* by the fitting function,

$$\ln \varepsilon_i = \sum_m P_m \ (\ln E_i)^{m-1} \tag{4.3}$$

Where, ε_i is the efficiency value considered for the cross section calculations, P_m is the fitting parameter of order *m* determined by fitting the above function to the measured efficiencies of ^{152}Eu source with their uncertainties propagated from four attributes *C*, I_γ, A_0 and λ. The total uncertainties due to these four attributes were determined using quadratic sum formula,

$$\left(\frac{\Delta\varepsilon_i}{\varepsilon_i}\right)^2 = \left(\frac{\Delta C_i}{C_i}\right)^2 + \left(\frac{\Delta I_{\gamma i}}{I_{\gamma i}}\right)^2 + \left(\frac{\Delta A_0}{A_0}\right)^2 + (t\Delta\lambda)^2 \tag{4.4}$$

Where, ΔC_i, $\Delta I_{\gamma i}$ *and* A_0 are the uncertainties in counts, γ-ray intensities and source activities respectively, and $\Delta\lambda = 0.693 \times \Delta T_{1/2}/T_{1/2}^2$ is the uncertainty in the decay constant.

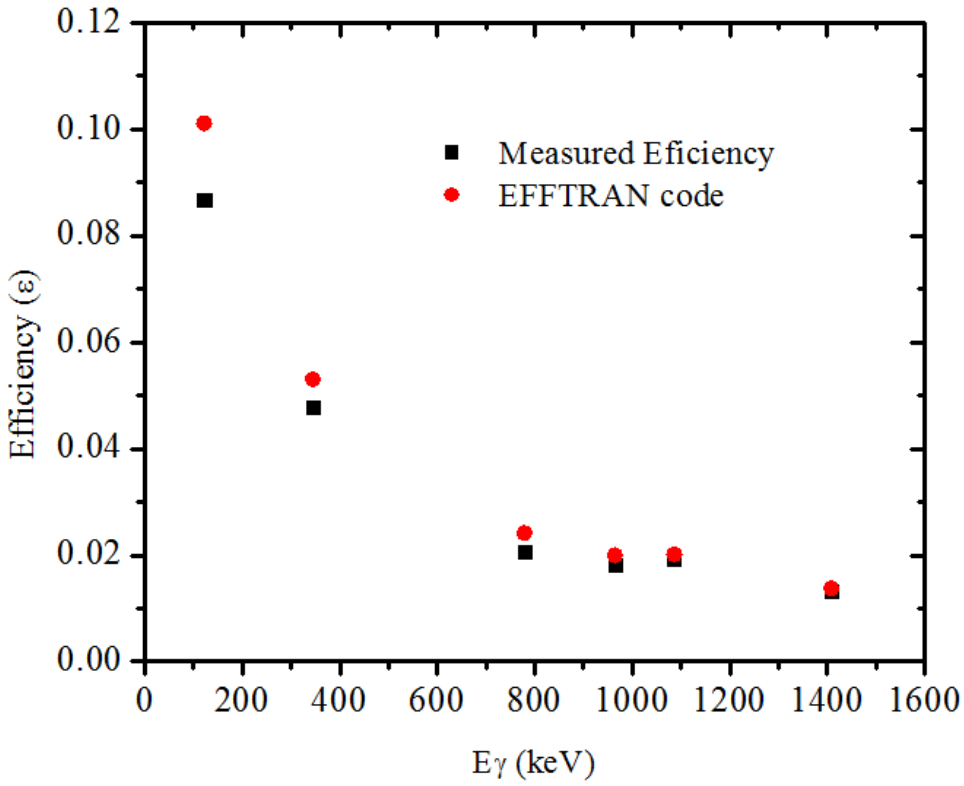

Figure 4.4 Comparison between the measured efficiency and EFFTRAN corrected efficiency

The partial uncertainties values are given in *Table 4.5* to create the covariance matrix for the detector efficiencies using formula,

$$(V_\varepsilon)_{ij} = \sum_r e_{ir} S_{ijr} e_{jr} \tag{4.5}$$

Where, e_{ir} and e_{jr} are the n × n diagonal matrices and S_{ijr} are the n × n micro-correlation matrix. The partial uncertainties of four attributes were given in *Table 4.5.* The covariance and correlation matrix for the HPGe detector efficiency were given in *Table 4.6.* The total error in the measured efficiencies is determined by the formula $\sigma_{\varepsilon ij} = (V_{\varepsilon ij})^{1/2}$. The above Eq. (4.3) can be written as Z=AP, with fitting parameters P_m and the corresponding covariance matrix *Vp* is given as ,

$$V_p = (A^T V_Z^{-1} Z) \text{ and } P_m = (A^T V_Z^{-1} Z) \tag{4.6}$$

Where V_Z is calculated by,

$$V_Z = \frac{\left(V_{\varepsilon_{ij}}\right)}{<\varepsilon_i><\varepsilon_j>}$$

Where, $V\varepsilon$ is the covariance matrix for the corresponding efficiencies ε, A is the design matrix with $A_i = (\ln E_i)^{m-1}$, m = 1,2,..k, i = 1,2,..6 and Z is the column matrix with $Z_i = \ln\varepsilon_i$ [34]. The best fit can be obtained as, $\chi^2_m = (Z - AP)' V_Z^{-1} (Z - AP)$. The best fit of the model in present work was obtained for m=5 with the goodness of fit $\chi^2_m = 0.177$ and fitting parameters values were P = -3.9537, -0.9343, -0.0592, -0.1476, -0.0722. From above fitting parameters, the interpolated efficiency for the characteristics γ-ray energies of product nuclei of the sample (^{187}W) and monitor (^{115m}In) with its uncertainties and correlation matrix were given in *Table 4.7*.

Table 4.5 Partial uncertainties of attributes to obtain HPGe detector efficiency

Eγ (keV)	C_{obs} (×10^{-4})	I_γ (×10^{-4})	A_0 (×10^{-4})	$T_{1/2}$ (×10^{-4})
121.78	1.384	5.659	12.39	8.890
344.27	3.256	3.975	6.476	4.648
778.90	2.230	1.492	2.959	2.123
964.07	3.085	0.955	2.444	1.754
1085.86	2.445	0.865	2.165	1.554
1408.01	2.168	0.588	1.684	1.208

Table 4.6 Covariance and correlation matrices for HPGe detector efficiency

Eγ (keV)	Covariance matrix (×10^{-7})						Correlations					
121.78	26.66						1.					
344.27	12.16	8.994					0.785	1.				
778.90	5.554	2.903	2.046				0.752	0.677	1.			
964.07	4.587	2.398	1.095	1.948			0.637	0.573	0.549	1.		
1085.86	4.639	2.425	1.108	0.915	1.803		0.669	0.602	0.577	0.488	1.	
1408.01	3.160	1.652	0.754	0.623	0.631	0.934	0.633	0.569	0.546	0.462	0.486	1.

Table 4.7 Interpolated detector efficiency of the characteristic γ-ray energies of the monitor and sample reactions with its uncertainties and correlation matrices

Reaction	Eγ (keV)	Efficiency	Correlations	
$^{115}In(n,n')^{115m}In$	336.24	0.05412 ± 0.00100	1.	
$^{186}W(n,\gamma)^{187}W$	479.53	0.03831 ± 0.00102	0.387	1.

4.3.2 Estimation of $^{186}W(n,\gamma)^{187}W$ reaction cross sections

The spectrum averaged cross section of $^{186}W(n,\gamma)^{187}W$ reaction was determined in the neutron energy range 0.60 MeV to 3.20 MeV using the method of activation and offline γ-ray spectrometry. The reaction cross section was measured by irradiating the target samples and measuring the counts of the selected characteristic γ-ray energies using the standard activation formula,

$$< \sigma_r > = < \sigma_m > \eta \frac{A_r \lambda_r a_m N_m I_m f_m}{A_m \lambda_m a_r N_r I_r f_r} \times \frac{C_r * N_{Corr\,(r)}}{C_m * N_{Corr\,(m)}} \qquad (4.7)$$

Where, $A_{r,m}$ is the photo-peak counts of product nuclei ^{187}W and ^{115m}In recorded by HPGe detector, $\lambda_{r,m}$ is the decay constant (cm^{-1}), $N_{r,m}$ is the total number of atoms , η ($\varepsilon_m/\varepsilon_r$) is the detector efficiency ratio, $\varepsilon_{r,m}$ is the efficiency of corresponding γ-ray energies of sample and monitor reaction, $I_{r,m}$ is the γ-ray intensity, $a_{r,m}$ is the isotopic abundance of the target and monitor nuclei and $f_{r,m}$ is the timing factors of the sample and monitor reaction are given by:

$$f_{r,m} = \left(1 - e^{-\lambda t_{irr}}\right) e^{-\lambda t_{cool}} \left(1 - e^{-\lambda t_{count}}\right) \qquad (4.8)$$

Where, t_{irr} is the irradiation time, t_{cool} is the cooling time which is the time difference when the irradiation stop and the counting started time and t_{count} is the counting time. $C_{r,m}$ is the total correction factor due to self-absorption of γ-rays, counting geometry and flux attenuation. $N_{corr\,(r,m)}$ is the low energy (p,n_1) neutron correction factor.

The partial uncertainties from each attribute in above Eq. (4.7) can be communicated directly to the sample cross section using the quadratic sum formula. The decay constant because of its relation to the cross section by an exponential function, the uncertainty in time factor (*f*) can be denoted as,

$$\left(\frac{\Delta f}{f}\right)^2 = \left(\frac{\lambda t_i e^{-\lambda t_i}}{1-e^{-\lambda t_i}} - \lambda t_c + \frac{\lambda(LT)e^{-\lambda(LT)}}{1-e^{-\lambda(LT)}} - 1\right)\left(\frac{\Delta\lambda}{\lambda}\right)^2 \quad (4.9)$$

The uncertainty in the detector efficiency for both sample and monitor reactions can be reduced by introducing $\eta_{m,s} = \frac{\varepsilon_m}{\varepsilon_s}$ as,

$$\frac{\Delta\eta_{m,r}}{\eta_{m,r}} = Var(\varepsilon_m) + Var(\varepsilon_r) - 2Cov(\varepsilon_m, \varepsilon_r) \quad (4.10)$$

and the obtained η value with its uncertainty is = 1.4128 ± 0.00112. The spectrum averaged cross section for the monitor reaction $<\sigma_m>$ is determined by the equations,

$$< \sigma_m > = \frac{\int_{Ej,min}^{Ej,max} \Phi_i \sigma_m dE}{\int_{Ej,min}^{Ej,max} \Phi_i dE} \quad (4.11)$$

Where, σ_m is the $^{115}In(n,n')^{115m}In$ monitor reaction cross section taken from the IRDFF-1.05 (International Reactor Dosimetry and Fusion File) library [35] folded with the neutron flux values (Φ_i) from the neutron flux energy spectrum generated by simulation code EPEN [25, 26]. $E_{j,min}$ and $E_{j,max}$ are the lower and upper energy values of the energy spectrum. The neutron flux calculated from monitor reaction was 2.627×10^6 n cm^2 s^{-1} at 0.61 ± 0.01 MeV, 4.151×10^6 n cm^2 s^{-1} at 2.11 ± 0.02 MeV and 3.621×10^6 n cm^2 s^{-1} at 3.13 ± 0.02 MeV neutron energies, respectively by considering correction factors.

The correlation coefficients for the monitor reaction are obtained using the equation,

$$Corr\ (< \sigma_i >< \sigma_j >) = \frac{Cov(<\sigma_i><\sigma_j>)}{\sqrt{Var<\sigma_i>}\sqrt{Var<\sigma_j>}} \quad (4.12)$$

The monitor spectrum averaged cross section with uncertainties and correlation matrix is given in *Table 4.8.*

Table 4.8 Spectrum averaged cross section with its uncertainty and correlation matrices

Reaction	En (MeV)	Cross section $<\sigma_m>$ (mb)	$\Delta<\sigma_m>$ (%)	Correlations		
$^{115}In(n,n'\gamma)^{115m}In$	0.61	13.03 ± 0.43	3.30	1.		
	2.11	295.87 ± 7.79	2.63	0.2759	1.	
	3.13	338.42 ± 8.04	2.38	0.2982	0.3390	1.

Correction factors

In the present study, the corrections are required in the measured cross section values to determine the actual cross section from the neutron photo-peak. Many factors play a role in determining the final values of the measured cross section. The correction factors of the experiment involved the γ-ray self-absorption factor of the sample at a given γ-energy (C_s), the flux attenuation factor (C_a), the counting geometry factor (C_g) and correction in measured cross section due to lower energy neutrons (N_{corr}) [36, 37].

In the present experiments, the radio activities in irradiated samples are uniformly distributed. The characteristic γ-rays from the sample of a certain thickness causes the γ-ray self-absorption effect due to the Photoelectric effect, the Compton effect and the Electron pair production effect. The correction factor was measured by the equation,

$$C_s = \frac{\mu_s t_s}{1-exp^{(-\mu_s t_s)}} \tag{4.13}$$

Where, t_s is a sample thickness (cm); μ_s is a mass absorption co-efficient (cm^2gm^{-1}) which determined from NIST-XCOM [38].

After the irradiation is completed, the samples were cooled for sufficient time and placed on a Perspex plate for γ-ray counting. The distance between the samples and the detector cap was kept in such a way that the coincidence summing effect was minimized during the counting time. The counting geometry correction factor (C_g) was calculated by,

$$C_g = \frac{(h+ d/2)^2}{h^2} \tag{4.14}$$

Where, d is the sample thickness (cm); h is the distance from the sample surface to the effective detection cross section of the crystal in the HPGe detector (cm).

Table 4.9 Correction factors in the present experiment

E_n (MeV)	$\frac{C_{s\,(r)}}{C_{S\,(m)}}$	$\frac{C_{g\,(r)}}{C_{g\,(m)}}$	$\frac{C_{a\,(r)}}{C_{a\,(m)}}$	C_r
0.61 ± 0.01	0.98374	0.98209	0.9999	0.96613
2.11 ± 0.02	0.98374	0.98209	0.9999	0.96613
3.13 ± 0.02	0.98374	0.98209	0.9999	0.96612

When the energetic neutrons travel through a sample of a certain thickness, because of the effect of flux attenuation these neutrons are absorbed by nuclear reactions. The correction factor for flux attenuation is measured by dividing the sample thickness into average k parts. Each part of the sample will produce the amount of radioactivity called N_1, N_2, N_3… N_k. The flux attenuation correction factor was derived by the following formula,

$$C_a = \frac{kN_1}{\sum_{i=1}^{i=k} N_i} \tag{4.15}$$

Where, N_i is the amount of radioactivity produced by i-th part of the sample. The correction factor due to experimental geometry is so insignificant that could be ignored. The total correction factor C_{tot} for sample reaction and monitor is calculated by the following formula and shown in *Table 4.9.*

$$C_{tot} = \frac{(C_s C_g C_a)_r}{(C_s C_g C_a)_m} \tag{4.16}$$

Table 4.10 Low neutron energy correction (N_{corr}) and γ-ray self-attenuation coefficient of sample and monitor reactions

Reaction	E_n (MeV)	N_{corr}	E_γ (keV)	C_s
	0.61 ± 0.01	0.98929		
$^{186}W(n,\gamma)^{187}W$	2.11 ± 0.02	0.88682	479.53	1.01416±0.00045
	3.13 ± 0.02	0.92766		
	0.61 ± 0.01	0.99998		
$^{115}In(n,n')^{115m}In$	2.11 ± 0.02	0.92434	336.241	1.02575±0.00130
	3.13 ± 0.02	0.94277		

As the proton energies are higher than the threshold energy of the reaction, the contribution of lower energy background neutrons from $^{7}Li(p,n_1)^{7}Be^*$ reaction was subtracted from measured $^{186}W(n,\gamma)^{187}W$ reaction cross section values and is calculated by the equation:

$$N_{corr} = 1 - \frac{\int \Phi_1(E)\sigma_x(E)dE}{\int \Phi(E)\sigma_x(E)dE} \tag{4.17}$$

Where, $\Phi_1(E)$ is the neutron flux energy spectrum for (p,n_1) neutrons and $\Phi(E)$ is the total cross section $[\Phi(E) = \Phi_0(E) + \Phi_1(E)]$ calculated by EPEN code. $\sigma_x(E)$ is the cross section values of

$^{186}W(n,\gamma)^{187}W$ reaction taken from ENDF/B-VIII.0 [8] and $^{115}In(n,n'\gamma)^{115m}In$ reaction cross section values taken from IRDFF-1.05 data library [17]. *Table 4.10* shows the calculated values of low energy corrections and the γ-ray self-absorption correction factors of associated γ-ray energies of sample and monitor reactions.

Covariance analysis and uncertainty propagation in cross section

The covariance matrix ($V_{(cs)ij}$) for reaction cross section was determined by considering the fractional uncertainty (%) of different attributed involved in the calculations (Eq. (4.7)). The fractional uncertainties (%) of the attributes considered to estimate the reaction cross sections as shown in *Table 4.11*. The measured $^{186}W(n,\gamma)^{187}W$ reaction cross section with their uncertainties, covariance and correlation matrix are presented in *Table 4.12*.

Table 4.11 Fractional uncertainties (%) of different attributed involved in present experiment

Attributes	Fractional Uncertainty (%)			Correlation
	En = 0.61±0.01 MeV	En = 2.11±0.02 MeV	En = 3.13±0.02 MeV	
A_r	8.6678	7.0995	6.2248	0
A_m	4.5380	0.6080	0.5895	0
η	0.0789	0.0789	0.0789	1
I_r	1.5038	1.5038	1.5038	1
I_m	0.2179	0.2179	0.2179	1
f_r	0.0860	0.0889	0.0674	1
f_m	0.0054	0.0077	0.0014	1
W_r	0.0353	0.0319	0.0334	0
W_m	0.0400	0.0363	0.0423	0
σ_m	3.3001	2.6329	2.3757	1
a_r	0.0352	0.0352	0.0352	1
a_m	0.01045	0.01045	0.01045	1

Table 4.12 Measured cross section with uncertainties, covariance and correlation matrices

En (MeV)	Cross section $<\sigma_s>$ (mb)	Covariance matrix			Correlations		
0.61 ± 0.01	46.618 ± 4.877	0.0109			1.		
2.11 ± 0.02	26.396 ± 2.043	0.000232	0.005988		0.02877	1.	
3.13 ± 0.02	19.474 ± 1.335	0.000232	0.000232	0.004700	0.03244	0.04378	1.

4.4 Theoretical calculations

The theoretical calculations of $^{186}W(n,\gamma)^{187}W$ reaction cross section were done by TALYS-1.9 and EMPIRE-3.2.2 nuclear codes [19, 20]. Both codes comprise various nuclear models, compound nucleus, level density and pre-equilibrium models, γ-ray strength functions across a wide range of energies and incident particles. Theoretical reaction cross sections was determined by combination of different input parameters, such as optical models, nuclear level densities and γ-ray strength functions within 0.4 to 5.0 MeV neutron energy range. The calculated reaction cross sections data were then compared to the present experimental results, the previously reported data from EXFOR database [18] and data available in ENDF/B-VIII.0,JEFF-3.3 and JENDL-5 [21-23] data library.

In EMPIRE-3.2.2 nuclear code, the optimized input parameters were utilized to investigate the $^{186}W(n,\gamma)^{187}W$ reaction cross section theoretically. Using parity dependent Hartree-Fock-Bogoliubov method (HFBM) of level density parameter, the capture cross section was predicted [39]. The γ-ray transmission coefficients was calculated from the default γ-ray strength function (GSTRFN=1) [40]. Also the width fluctuation correction was applied with the Hofmann, Richert, Tepel and Weidenmuller (HRTW) model up to 5 MeV [41]. The capture cross section in the EMPIRE code was calculated using the exciton model (PCROSS=1.5) and the default optical model potential (OMPOT=2408) [42].

The $^{186}W(n,\gamma)^{187}W$ reaction cross sections have been calculated by Talys-1.9 code taking into account the level density models with optimal values of input parameters in the neutron energy range from 4 to 20 MeV. In the present case, Skryme-Hartree-Fock-Bogoluybov different level density models (LDMODEL 4) was considered for estimation of reaction cross section with other optimized input parameters [43]. The code takes into account

the direct, pre-equilibrium and compound components of the cross section in the calculations. The Brink-Axel Lorentzian model (strength-2) has been used for the γ-ray strength function [44]. In TALYS, in order to calculate the reaction cross sections, different input parameters like nuclear models, level densities, decay schemes and other input parameters are taken from the Reference Input Parameter Library RIPL-3 database [45].

4.5 Results and discussion

The $^{186}W(n,\gamma)^{187}W$ reaction cross sections with uncertainties, covariance and correlation matrices were presented in *Table 4.12* at spectrum averaged neutron energies of E_n=0.61 ± 0.01, 2.11 ± 0.02 and 3.13 ± 0.02 MeV using activation and offline γ-ray spectrometric technique. The comparison between the measured cross sections with the previously published data was presented in *Table 4.13* and the data from TALYS-1.9, EMPIRE-3.2, ENDF/B-VIII.0, JEFF-3.3 and JENDL-5 [19-23] were presented in *Figure 4.5*. The available data were published few decades ago have scarcity due to discrepancies in the decay data and monitor cross sections. The comparison with evaluated data shows that the cross section data with ENDF-V.III.0 [21] data library agrees at 0.61 ± 0.01 MeV (46.49 mb) and 3.13 ± 0.02 MeV (17.049 mb) data and underestimates at 2.11 ± 0.02 MeV (29.38 mb). From *Figure 4.5*, it is observed that the measured cross section data are in good agreement with the data predicted by EMPIRE-3.2 at 0.61 ± 0.01 MeV (43.87 mb); at 2.11 ± 0.02 MeV (29.15 mb) and 3.13 ± 0.02 MeV (25.45 mb) while the measured data are underestimates for TALYS-1.9 data except at 3.13 ± 0.02 MeV (21.43 mb). The comparison with the previously reported data indicated that the measured cross section data agrees with reported data by M. Lindner et al. [10] at 0.6 MeV (48 mb) and data reported by G. G. Zaikin et al. [12] at 2.11 MeV (29.1 mb) and 3.11 MeV (23.1 mb).

Table 4.13 Comparison of measured $^{186}W(n,\gamma)^{187}W$ reaction cross section with previously reported data

En (MeV)	Cross section $\langle\sigma_s\rangle$ (mb)	*Literature*		
		En (MeV)	*$\langle\sigma_s\rangle$ (mb) with ref.*	
0.61 ± 0.01	46.618 ± 4.877	0.6	48	M. Lindner et al. (1976)
		0.595	45	A.E. Johnsrud et al. (1959)
2.11 ± 0.02	26.396 ± 2.043	2.11	29.1	G.G. Zaikin et al. (1968)
3.13 ± 0.02	19.474 ± 1.335	3.11	23.1	G.G. Zaikin et al. (1968)
		3.1	16	J.A. Miskel et al. (1962)
		3.1	24	A.E. Johnsrud et al. (1959)

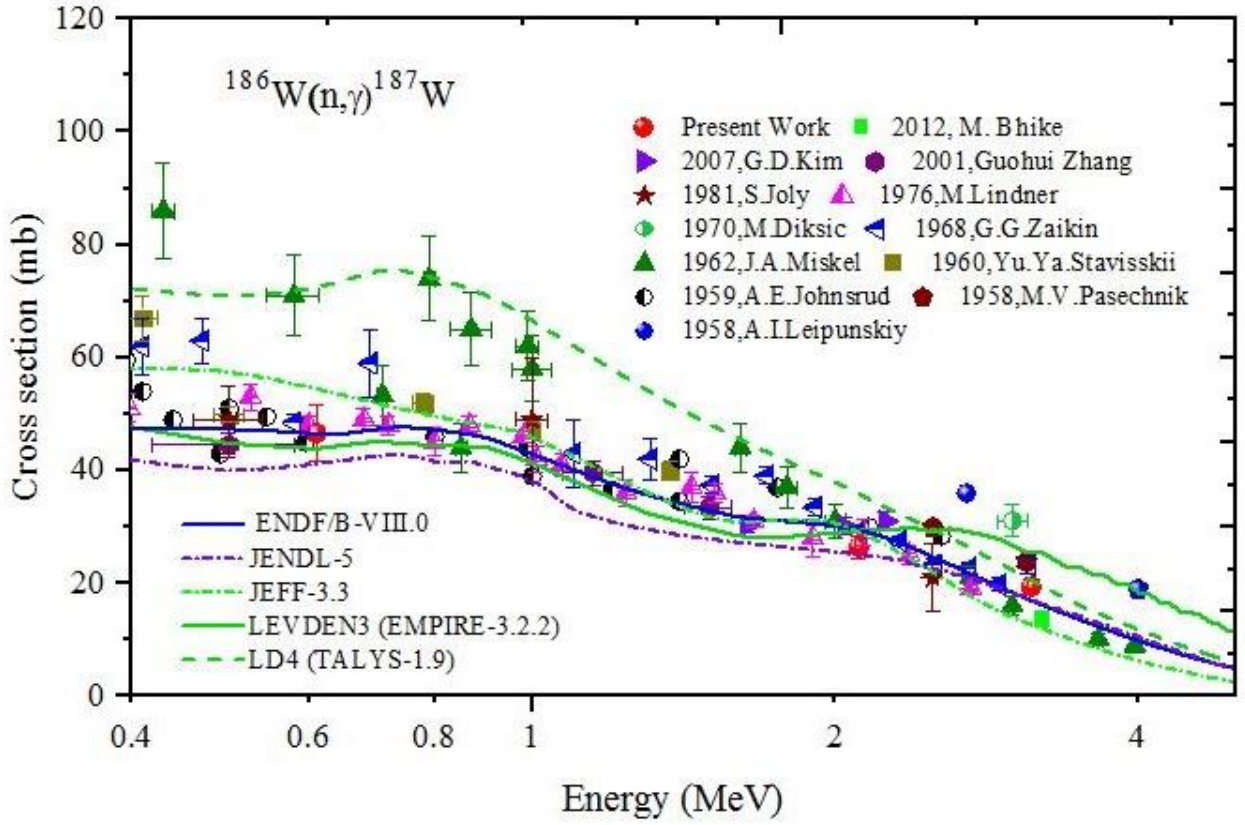

Figure 4.5 Comparison of $^{186}W(n,\gamma)^{187}W$ reaction cross section with previously published data, evaluated data and theoretical data

4.6 Conclusion

The cross section of $^{186}W(n,\gamma)^{187}W$ reaction was measured at spectrum averaged neutron energies 0.61 ± 0.01 MeV; 2.11 ± 0.02 MeV and 3.13 ± 0.02 MeV, and the measured values are 46.618 ± 4.877 mb, 26.396 ± 2.043 mb and 19.474 ± 1.335 mb, respectively. A detailed analysis of uncertainties propagated by various attributes was resented with covariance and correlation matrices. The measured values are compared with the literature data, theoretically predicted data by TALYS-1.9 and EMPIRE-3.2 codes and evaluated data from ENDF/B-VIII.0, JEFF-3.3 and JENDL-5. The measured results are in good agreement with the ENDF/B-VIII.0 and EMPIRE-3.2 data as well as the data reported earlier.

References

[1]. B. I. Khripunov, V. S. Koidan, A. I. Ryazanov, V. M. Gureev, S. N. Kornienko, S. T. Latushkin, A. S. Rupyshev, E. V. Semenov, V. S. Kulikauskas, V. V. Zatekin, Physics Procedia 71 (2015) 63-67.

[2]. Yousry Gohar, Igor Bolshinsky, Ivan Karnaukhov, KIPT accelerator-driven system design and performance, Report No. NEA/NSC/DOC (2015) 7.

[3]. R. A. Forrest, Fusion Engineering and Design 81 (18) (2006) 2143-2156.

[4]. T. Kawano, M. B. Chadwick, P. Talou, P. G. Young, and L. Bonneau, Nuclear Reaction Data for Nuclear Technologies and Applications, AIP Conference Proceedings 1005 (2008) 17.

[5]. J. Marganiec, I. Dillmann, C. Domingo Pardo and F. Kappeler, Physical Review C 80 (2009) 025804.

[6]. M. Bhike, B. J. Roy, A. Saxena, R. K. Choudhury, S. Ganesan, Nuclear Science and Engineering,170 (2012) 44.

[7]. G. D. Kim, H. J. Woo, H. W. Choi, N. B. Kim, T. K. Yang, J. H. Chang, K. S. Park, Journal of Radioanalytical and Nuclear Chemistry, 271 (2007) 553.

[8]. Guohui Zhang, Zhaomin Shi, Guoyou Tang, Jinxiang Chen, Guangzhi Liu, Hanlin Lu, Nuclear Science and Engineering, 137 (2001) 107.

[9]. J. Voignier, S. Joly, G. Grenier, D.M. Drake, L. Nilsson, Report: Centre d`Etudes Nucleaires, Saclay ReportsNo.5089, NSR-Key No: 1981VOZW (1981).

[10]. M. Lindner, R. J. Nagle, J. H. Landrum, Nuclear Science and Engineering 59 (1976) 381.

[11]. M. Diksic, P. Strohal, G. Peto, P. Bornemisza-Pauspertl, I. Hunyadi, J. Karolyi, Acta Physica Hungarica, 28 (1970) 257.

[12]. G. G. Zaikin, I. A. Korzh, N. T. Sklyar, I. A. Totskii, Soviet Atomic Energy 25 (1968) 1362.

[13]. J. A. Miskel, K. V. Marsh, M. Lindner, R. J. Nagle, Physical Review 128 (1932) 2717.

[14]. Yu.Ya. Stavisskii, V.A. Tolstikov, Journal of Nuclear Energy A&B (Reactor Sci. and Technol.) 16 (1960) 496.

[15]. A. E. Johnsrud, M. G. Silbert, H. H. Barschall, Physical Review 11 (1959) 927.

[16]. M. V. Pasechnik, I. F. Barchuk, I. A. Totskiy, V. I. Strizhak, A. M. Korolev, Yu. V. Gofman, G. N. Lovchikova, E. A. Koltypin, G. B. Yankov, Conf.: Second Internat. At. En. Conf., Geneva, Vol.15 (1958) 18.

[17]. A. I. Leipunskiy, O. D. Kazachkovskiy, G. Ja. Artyukhov, A. I. Baryshnikov, T. S. Belanova, V. I. Galkov, Yu. Ja. Stavisskiy, E. A. Stumbur, L. E. Sherman, Conf.: Second Internat. At. En. Conf., Geneva, Vol.15 (1958) 50.

[18]. EXFOR, Cross Section Information Storage and Retrieval System (EXFOR), IAEA, Vienna, Austria, http://www.nds.iaea.or.at/exfor/(online)

[19]. A. J. Koning, S. Hilaire, M. C. Duijvestijn, TALYS-1.9, in Proceedings of the International Conference on Nuclear Data for Science and Technology, April 22-27, 2007, Nice, France, editors O. Bersillon, F. Gunsing, E. Bauge, R. Jacqmin, and S. Leray, (EDP Sciences, Les Ulis, France 2008) 211.

[20]. M. Herman et al., EMPIRE-3.2 Malta modular system for nuclear reaction calculations and nuclear data evaluation User's Manual, No. BNL [101378-2013]. Brookhaven National Laboratory (BNL) National Nuclear Data Center, (2013).

[21]. D. A. Brown et al., Nucl. Data Sheets 148 (2018) 1.

[22]. https://www.oecd-nea.org/dbdata/jeff/jeff33/

[23]. A. J. M. Plompen et al., Eur. Phys. J. A 56 (2020) 1.

[24]. P. Singh et al, Pramana Journal of Physics 59 (2002) 739.

[25]. R. Pachuau et al., Nucl. Sci. Eng. 187 (2017) 70.

[26]. R. Pachuau et al., EPJ Web Conf. 146 (2017) 12016.

[27]. M. J. Martin, Nuclear Data Sheets 114 (2013) 1497-1847.

[28]. NuDat 3.0 (2023) National Nuclear Data Center, Brookhaven National Laboratory. http://www.nndc.bnl.gov/nudat3

[29]. M. S. Basunia, Nuclear Data Sheets, 110 (5) (2009) 999-1238.

[30]. Jean Blachot, Nuclear Data Sheets, 113(10) (2012) 2391-2535.

[31]. J. J. Griffin, Phys. Rev. Lett., 17 (1966) 478.

[32]. T. Vidmar, Nuclear Instruments Methods A 550 (2005) 603.

[33]. T. Vidmar, G. Kanisch, G. Vidmar, Applied Radiation and Isotopes 908 (2011) 69.

[34]. L. P. Geraldo, Nucl. Instrum. And Methods in Phys. Res. A 290 (1990) 499-508.

[35]. E. M. Zsolnay, R. Capote, H. K. Nolthenius, A. Trkov, International Atomic Energy Agency Technical Report No. INDC(NDS)-0616 (2012).

[36]. Su Shen, Zhiling Yuan, Xiaobing Luo, Nuclear Inst. and Methods in Physics Research B 476 (2020) 59-63.

[37]. A. Gandhi, Aman Sharma, Rebecca Pachuau, B. Lalremruata, Mayur Mehta, Prashant N. Patil, S. V. Suryanarayana, L. S. Danu, B. K. Nayak, A. Kumar, Eur. Phys. J. A, 57 (1) (2021).

[38]. M. J. Berger; J. H. Hubbell, S. M. Seltzer, J. Chang; J. S. Coursey; R. Sukumar; D. S. Zucker, K. Olsen. XCOM: photon cross sections database, NIST standard reference database (XGAM), 2010. Available at http://www.nist.gov/pml/data/xcom/index.cfm

[39]. S. Goriely, M. Samyn, and J. M. Pearson, Phys. Rev. C 75 (2007) 064312.

[40]. D. M. Brink, Ph.D. thesis, Oxford University (1955).

[41]. H. M. Hofmann et al., Ann. Phys. 90 (1975) 403.

[42]. J. J. Griffin, Phys. Rev. Lett. 17 (1966) 478.

[43]. A. V. Ignatyuk, J. L. Weil, S. Raman, S. Kahane, Phys. Rev. C 4(1993)71504.

[44]. D. M. Brink, Nucl. Phys. 4, 215 (1957); P. Axel, Phys. Rev. 126 (1962) 671.

[45]. R. Capote, M. Herman, P. Oblozinsky, et al., Nucl Data Sheets 110 (2009) 3107.